Carbohydrate Polymers 112 (2014) 376–386

Contents lists available at ScienceDirect

Carbohydrate Polymers

journal homepage: www.elsevier.com/locate/carbpol

Transdermal delivery of 10,11-methylenedioxycamptothecin by hyaluronic acid based nanoemulsion for inhibition of keloid fibroblast

Yuanyuan Gao[a], Xiaojie Cheng[a], Zhiguo Wang[b], Juan Wang[a], Tingting Gao[a], Peng Li[b], Ming Kong[a,*,1], Xiguang Chen[a,*,1]

[a] College of Marine Life Science, Ocean University of China, Yushan Road, Qingdao 266003, Shandong, China
[b] Department of Plastic Surgery, The Affiliated Hospital of Medical College Qingdao University, Qingdao 266013, Shandong, China

ARTICLE INFO

Article history:
Received 23 February 2014
Received in revised form 3 May 2014
Accepted 5 May 2014
Available online 2 June 2014

Keywords:
Hyaluronic acid
Nanoemulsion
10,11-Methylenedioxycamptothecin
Transdermal delivery
Keloid fibroblast

ABSTRACT

This study designs an alternative transdermal delivery system for 10,11-methylenedioxycamptothecin(MD-CPT) to inhibit keloid. Hyaluronic acid nanoemulsions (HANs) with nano size, negative charge and good stability were prepared as transdermal carriers. The MD-CPT loaded HANs performed desirable skin permeable capacity across human keloid skin and the drug was transferred directly to keloid lesion area. MD-CPT was delivered percutaneously higher than the control group. FITC-HANs could be successfully internalized by keloid fibroblast (KF) and deliver MD-CPT toward nucleus, inhibited the proliferation of KF, while there was no serious toxicity to normal skin fibroblasts. The growth-inhibitory effect was further clarified upon cell cycle regulation, which arrested cells at G1/S and prevented them entry into mitosis. KF gene expression demonstrated plasminogen activator inhibitor-1 (PAI-1) was significantly down-regulated and Smad7 up-regulated, which was beneficial to inhibit keloid. The study demonstrated that as transdermal delivery of MD-CPT by HANs has potential for inhibition of keloid fibroblast.

1. Introduction

Keloid disease (KD) is recognized as benign tumor characterized by fibroblastic proliferation (Syed, Bagabir, Paus, & Bayat, 2013). Although the pathogenesis is not clear, the diagnostics research of KD and hypertrophic scar has made great progress and the formation of KD is periodic (Tuan & Nichter, 1998; Bayat, Arscott, Ollier, Mc Grouther, & Ferguson, 2005). At KD formation initial stage, Keloid possess cancer-like properties, with overproliferation of keloid fibroblast, gradually invasion and migration to surrounding tissue, increased angiogenesis, and overexpression of cytokine like transforming growth factor-β (TGF-β), plasminogen activator inhibitor (PAI-1), specially for new wound healing of KD excision (Shih & Bayat, 2010).

Camptothecin (CPT), an anti-tumor agent, has attracted significant interests in hyperplastic cells due to its unique mechanism that it inhibits type I DNA topoisomerase (Top I). CPT analogues correlate with the drug-induced accumulation of Top I-DNA cleavable complexes and with inhibitory activity against DNA relaxation by Top I (Kano et al., 1992). 10,11-Methylenedioxycamptothecin (MD-CPT) as an important CPT analogue is of particular interest because it is capable of forming a covalent complex with DNA through nucleophilic displacement of the chlorine moiety by DNA while it is in the cleavable complex, which shows a longer lifetime and better stability for higher biological activity (Tanizawa, Kohn, Kohlhagen, Leteurtre, & Pommier, 1995; Supko & Malspeis, 1993). As a cell cycle specific agent, not all of the cells are susceptible to brief treatment with CPT analogues, but the CPT-induced apoptosis is selective to hyperplastic cells as G1/S Cell Cycle Blockers (O'Connor et al., 1991; Park, Morris, Greene, & Geller, 1997; Adams et al., 2006). Topical application of Hydroxycamptothecin (HCPT) could effectively prevent fibroblast proliferation and reduce epidural adhesion after laminectomy in rats (Sun et al., 2008).

However, CPT-based therapeutic agents still have limitations. These cytotoxic drugs also affect other rapidly dividing cells including cells in the gastrointestinal tract, bone marrow cells and hair follicles. Additionally, due to the hydrophobic nature of many chemotherapeutic drugs, parenteral administration via intravenous infusion typically requires the use of vehicles formulation (such as Cremophor EL). In addition, undesirable water-solubility of drug remains a challenge. Therefore, degradable hydrophobic

* Corresponding authors. Tel.: +86 0532 82032586; fax: +86 0532 82032586.
E-mail addresses: kongming@ouc.edu.cn (M. Kong), xgchen@ouc.edu.cn, qqsn160@163.com (X. Chen).
[1] These authors contributed equally to this manuscript as co-corresponding authors.

http://dx.doi.org/10.1016/j.carbpol.2014.05.026
0144-8617/

drug carriers are being developed to target and release drugs in a controlled fashion (Hariri et al., 2013).

Since the lesion area of keloid is the dermis, transdermal drug delivery formulations for direct administration are expected to create a permeating skin release of the drug across stratum corneum and diffuse deeper into dermis. In particular, alcohol-free oil/water hyaluronic acid nanoemulsions (HANs) have been applied as transdermal carriers for active hydrophobic ingredient, and using α-tocopherol as model ingredient, performed desirable skin permeable capacity via follicular and intercellular pathway without any chemical enhancers. No irritation has been found in dermis and skin surface (Kong, Chen, Kweon, & Park, 2011a, Kong, Chen, & Park, 2011b). Hyaluronic acid (HA) as one of the primary components of the nanoparticles, has a lot of available properties including specific viscoelasticity, biocompatibility, hydration and lubrication, and is often used as adjuvant of cosmetic surgery dressing, extremely attractive for various technologies concerned with body repair (Collins & Birkinshaw, 2013b). Meanwhile, hyaluronic acid is able to target to part hyperplastic tumor cells (Ganesh, Iyer, Morrissey, & Amiji, 2013). Furthermore, HANs can overcome the poor uptake of MD-CPT into keloid fibroblasts. The hydrophobic drug can be loaded into the hydrophobic kernel of nanoemulsion. The small size, flexible structure and hydrophilic interface facilitated transdermal permeation (Kong et al., 2013).

In the present study, we prepared and characterized HA based nanoemulsion loaded MD-CPT (MD-CPT/HANs). Through transdermal delivery, HANs transferred the hydrophobic MD-CPT into the dermis of the lesion area of keloid skin and inhibited the proliferation of keloid fibroblast, contributed to cell cycle arrest, prevented its entry into mitosis and inhibited the overexpression of the relevant cytokine. MD-CPT/HANs were verified as potential formulation to inhibit keloid fibroblast in this study.

2. Materials and methods

2.1. Reagents

Sodium forms of HA (M_w = 10 kDa), EDC (1-ethyl-3-(3-dimethylaminopropyl) carbodiimide), monostearin (glycerol α-monostearate, GMS) and *N*-hydroxy succinimide (NHS, 97%), methylene chloride, and Triton X-100 were purchased from Sigma Chemicals (Shanghai, China). Tween 80 and Span 20 were purchased from Solarbio (Beijing, China). 10,11-Methylenedioxycamptothecin (MD-CPT) was a gift of Tao Jiang research group, school of medicine and pharmacy, Ocean University of China. All the chemicals were analytical grade and were used as received. Keloid fibroblast (KF) and human skin fibroblast (HSF) obtained from primary culture of human tissue which was gifted by Department of Plastic Surgery, the Affiliated Hospital of Medical College Qingdao University. Wistar rats were purchased from Qingdao Municipal Institute for Drug Control.

2.2. Cell culture

Primary KF and HSF were cultured in DMEM (Dulbecco's modified Eagle's medium, Hyclone) in 10% FBS (Gibco), 100 U/mL penicillin, and 100 g/mL streptomycin within a humidified incubator containing 5% CO_2 at 37 °C and passed every 5–6 days to maintain logarithmic growth.

2.3. Preparation of HANs and MD-CPT/HANs

Amphiphilic HA-GMS was formulated by a previous method; GMS was conjugated to HA by formation of ester linkages through an EDC/NHS mediated reaction (Kong et al., 2011a,b; Collins & Birkinshaw, 2013b). HA nanoemulsions (HANs) were prepared through oil/water/surfactant (O/W/S) emulsifying system and solvent evaporation (Kong & Park, 2011). Briefly, HA-GMS PBS solution (pH7.4) was the continuous phase, methylene chloride as disperse phase, and Tween 80 and Span 20 (HLB = 12.5) as surfactants. The three components comprised in a mass ratio of 95/2/3. The disperse phase was added dropwise to a HA-GMS solution to form a coarse emulsion, which was further pulse-sonicated twice (pulse on, 10.0 s; pulse off, 2.0 s; 3 min/cycle; power 225 W), using 0.05% $CaCl_2$ as crosslinking agent. The methylene chloride was removed by a rotary vacuum evaporator at 35 °C, the suspension obtained was incubated in a water bath at 60 °C for 10 min to yield HANs. During preparation, MD-CPT was dissolved in the methylene chloride to obtain MD-CPT loaded HANs (MD-CPT/HANs), and the unloaded nanoemulsion was control, whose composition and formulation were exactly same except for MD-CPT. The Entrapment efficiency was the percentage fraction of the total drug incorporated into the nanoemulsion. Nanoemulsion was labeled with FITC as previous paper (Kong et al., 2013) (Ex 488 nm, Em 525 nm).

2.4. Particle size, zeta potential and surface morphology

Particle size of the HANs and MD-CPT/HANs was measured using dynamic laser scattering or photon correlation spectroscopy using a Malvern Zetasizer Nano ZS (Malvern Instruments, UK). For the measurements, MD-CPT/HANs were diluted with PBS prior to size measurement. The mean diameters of HANs and MD-CPT/HANs were monitored in Gaussian mode. Zeta potential of HANs and MD-CPT/HANs was measured using electrophoretic light scattering spectrophotometer (ELS 8000, Otsuka Electronics Co. Ltd., Japan). Surface morphology was examined by TEM (JEM-2010, Japan).

2.5. Physical stability of HANs

The physical stability of the HANs was investigated by monitoring both particle size and zeta potential during the storage at various time points (0, 1, 3, 7, 14, 28 days) after the preparation. The HANs from three batches were stored at 4 °C for 28 days. The HANs were diluted with filtered PBS to measure particle size and zeta potential.

The in vitro release study of HANs was performed by dialysis method in PBS (pH 7.4). The dialysis bags (molecular weight cut off 12–14 kDa) were rinsed with sufficient amount of water after boiling for 10 min in water. HANs and 0.25% carboxy methyl cellulose (CMC) suspension containing an equivalent to 2 mg of MD-CPT in PBS (pH 7.4) were placed in the activated dialysis bags. The dialysis fluid was PBS (pH 7.4) for 8 h. The media was agitated at 50 rpm and the temperature of the system was set at 37 ± 0.5 °C. The samples were withdrawn at predetermined time intervals and analyzed for fluorescent MD-CPT on the FLx8000 Biotek plate reader (Biotek, Winooski, Vermont) at excitation and emission wavelengths of 367 nm and 405 nm, respectively (Gorain et al., 2014). The accumulative release percentage (*Q*%) was calculated by the following equation, and the analyses were performed in triplicates.

$$Q\% = C_i V + \sum C_{i-1} V_s \quad (1)$$

where C_i is the MD-CPT concentration at T_i, V is the total volume of release medium, V_s is the sampling volume at T_i.

2.6. Cytotoxicity assays

Experimental samples included HA-GMS, MD-CPT and HA-GMS/MD-CPT (HA-GMS and MD-CPT were simultaneously added to the serum-free medium at ratio of 4:1 (m/m) and stired overnight to blend. Cell viability treated with experimental samples was determined using MTT assay. The cells were seeded at 1×10^3 cells/well

onto 96-well plates and incubated for 24 h. The culture medium was replaced by the serum-free medium with experimental sample after 24 h. At predetermined time, the cells were washed with PBS to remove the remained MTT and sample residues. Then the DMSO was added to dissolve the MTT formazan purple crystal. An enzyme-linked immunosor-bent assay (ELISA) reader was used to measure the absorbency of the solution at 490 nm in a microplate reader (MCC340, Multiskan, Belgium). The cell viability (%) was defined relative to untreated control cells.

$$\text{Cell viability } (\%) = \left[\frac{\text{OD}_{(\text{sample})}}{\text{OD}_{(\text{control})}}\right] \times 100 \quad (2)$$

where $\text{OD}_{(\text{sample})}$ and $\text{OD}_{(\text{control})}$ are the absorbances of the tested sample and the negative control sample.

2.7. Cellular uptake study

KFs were cultured in glass bottom cell culture dishes for confocal laser scanning microscope (inner diameter 35 mm) for 24 h to form a confluent monolayer. Then the culture medium was replaced by transport buffer (Hank' balanced salt solution, HBSS, pH7.4) and incubated at 37 °C for 30 min. After equilibration, the culture medium was changed with 100 μL of freshly prepared FITC-MD-CPT/HANs suspension (50–800 μg/mL in PBS) and incubated at 37 °C for 30 and 60 min. The nucleus was labeled with PI (propidium iodide, red fluorescence; λ_{Ex} 535 nm λ_{Em} 615 nm). The cells treated with MD-CPT/HANs were fixed with 4% paraformaldehyde for 15 min, stained with PI (Dyeing buffer contained RNase A.) The experiment was terminated by washing the cell monolayer three times with phosphate-buffered saline (PBS, pH7.4). The cells in the dish were viewed by confocal laser scanning microscope (Olympus, Tokyo, Japan) (Li et al., 2009).

2.8. Transdermal drug permeation study

2.8.1. Preparation of skin

Wistar rats were used (Male Wistar Rats weighting 200–250 g). The rat dorsal surface hairs were removed by a clipper and skin (full thickness) was surgically removed. The tissue (subcutaneous) was removed manually and dermis side was wiped with isopropyl alcohol (remove residual adhering fat). Thus full thickness of skin was washed with buffered (PBS), wrapped in foil (aluminum) and stored at −20 °C till further use (used within 2 weeks of preparation) (Chaudhary, Kohli, & Kumar, 2013).

2.8.2. Quantitative studies of transdermal drug permeation

Ex vivo permeation studies were carried out through rat skin using an automated transdermal diffusion cell sampling system (HC-268, Rightway Technology Co., LTD, China) with a diffusion area of 0.636 cm^2 and 5 mL receptor cell volume. The water was warmed with the built heater and then assembly was set thermostatically at 32 °C. A pump circulated the warmed water throughout the system. The receiver compartment was filled with PBS pH 7.4 and magnetically stirred at 800 rpm. The cumulative active ingredient penetration (Qt, μg/cm^2) through the skin was calculated from the following equation:

$$Qt = V_r C_t + \sum_{i=0}^{t-1} V_s C_i \quad (3)$$

where Ct is the drug concentration of the receiver solution at each sampling time, C_i is the drug concentration of the ith sample, and V_r and V_s are the volumes of the receiver solution and the sample, respectively. Data were expressed as the cumulative drug permeation per unit of skin surface area, Qt/S. The steady-state fluxes (J_{ss}, μg/(cm^2 h)) was calculated as below:

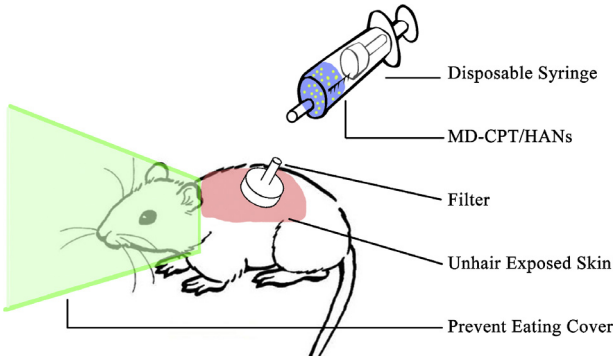

Fig. 1. Schematic diagram of rat transdermal delivery model.

$$J_{ss} = \frac{\Delta Qt}{\Delta t \times S} \quad (4)$$

where ΔQt is the cumulative drug permeation within certain period (Δt).

Apparent permeability coefficients (Kp, $\times 10^{-3}$ cm/h) were calculated according to the equation:

$$Kp = \frac{J_{ss}}{Cd} \quad (5)$$

where Cd is the active ingredient concentration in the donor compartment, and it assumed that under sink conditions the drug concentration in the receiver compartment is negligible compared to that in the donor compartment (Yang, Gao, Bao, Su, & Chen, 2013).

2.8.3. Qualitative studies of transdermal drug permeation

A recently developed ex vivo Keloid OC model was used (Bagabir, Syed, Paus, & Bayat, 2012). This keloid case with unambiguous typical clinical features belonged to a 27 years old male patient, and generated for approximately 1 year. The excised keloid tissue was washed and soaked in PBS for 30 min. Keloid tissues were cut into 3 mm punch biopsy sizes and embedded in rat tail collagen gel matrix at the air–liquid interface. Skin surfaces were treated with MD-CPT/HANs twice per day at dosage of 0.5 mL per time. MD-CPT/HANs were labeled with rhodamine (Ex 543 nm, Em 625 nm) as previous paper (Kong et al., 2011a,b). All procedures were carried out under light protection. Tissues were collected on 0, 4 and 24 h for observation by a fluorescence microscope (Olympus, Tokyo, Japan).

2.9. In vivo study of MD-CPT/HANs transdermal delivery

2.9.1. Rat model of MD-CPT/HANs transdermal delivery

Wistar rats (male, 4 weeks age, average weight: 200 g) were prepared. The rats were fasted to prevent food fluorescence interference in gastrointestinal tract. As is shown in the schematicdiagram (Fig. 1), the rat dorsal surface hair was removed by a clipper. The part of Swinnex Filter with Luer–Lok port (Swinnex ×13, Millipore USA) was fixed by super glue on the dorsal surface. The area of filter contact with skin is the effective area of transdermal drug delivery (1.33 cm^2, diameter 13 mm, thickness 10 mm) and so the maximum dose volume was 1.33 cm^3. The head of rat was covered to avoid bite and lick. Rats were treated with MD-CPT/HANs twice per day at dosage of 0.5 mL per time.

2.9.2. Tissue distribution of MD-CPT/HANs

Rats were treated with MD-CPT/HANS for 1 and 2 days; the other group without any treatment served as a control. Animals were

observed carefully for the onset of any signs of toxicity. After rats were killed, internal organs of each animal were collected immediately at various time points, weighted, and frozen at −20 °C until analysis. The parts of each organ were cut off and made into frozen section and viewed under a fluorescence microscope (Olympus, Tokyo, Japan). All excised tissues were further homogenized on ice in 1.5 mL PBS, and the resulting homogenates were analyzed for fluorescent MD-CPT on the FLx8000 Biotek plate reader as 2.5 the in vitro release study.

2.10. Cell cycle analysis

KFs were incubated with HA-GMS/MD-CTP for 12, 24 and 48 h (MD-CPT: 25 and 50 μg/mL). Cells were harvested and fixed in 70% ethanol overnight. After double washing with PBS, cells were labeled with 500 μL PI staining buffer (Sigma, Shanghai, China) and incubated at room temperature in the dark for 30 min. DNA content was analyzed using Gallios Flow Cytometer (Beckman, USA) (Hariri et al., 2013).

2.11. Gene expression

KFs and HSF were incubated with HA-GMS, MD-CTP for 24 h (HA-GMS 100 μg/mL, MD-CPT 25 μg/mL). Total RNA from control or treated fibroblasts were extracted (Trizol, Invitrogen) and analyzed by Real time PCR, using β-actin as internal standard (see Table 1 for primer sequences).

Table 1
Primers used for gene expression.

Primer name	Forward primer	Reverse primer
Smad3	TGGAGGGTGTAGTGGCTTTTTG	CGCGGCCACTTGTTTAGC
Smad7	CTGGGAGGGACATGCTTAGC	AGTTAGGTGTCAGCCTAGGATGGT
PAI-1	GACTCACAGCCGCATTGGT	TCACGTGTCCACTGCTCACA
TGF-β	TCTTTTGATGTCACCGGAGTTG	GCGAAAGCCCTCAATTTCC
β-Actin	CTGGAACGGTGAAGGTGACA	CGGCCACATTGTGAACTTTG

Sequence (5′ to 3′).

2.12. Statistical analysis

Each experiment was performed independently at least three or four times. Data are given as mean ± SEM. Statistical evaluation of the continuous data was performed using one-way analysis of variance, followed by Tukey test for between-group comparisons. Statistical analyses were performed using commercially available

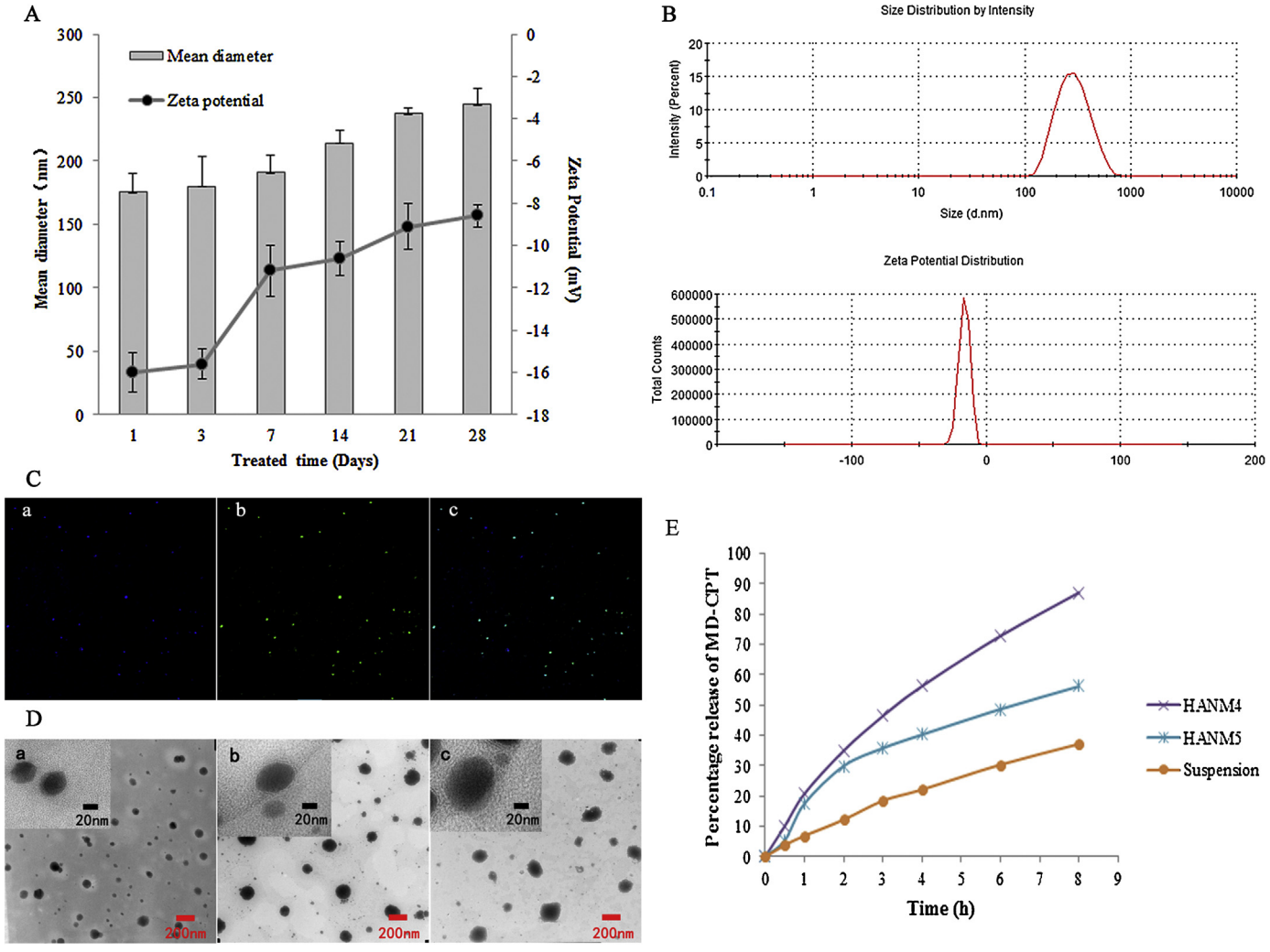

Fig. 2. (A) Physicochemical properties of MD-CPT/HANs (m/m 4:1) during the storage: particle size and zeta potential of MD-CPT/HANs. The results are expressed as mean ± SD (n = 3). (B) Size distribution and zeta potential of MD-CPT/HANs at the 28th day. (C) Fluorescence microscope photos of FITC-MD-CPT/HANs (400×): (a) MD-CPT (blue), (b) FITC-labeled HANs (green), and (c) MD-CPT/HANs MD-CPT/HANs (cyan). (D) TEM pictures of (a) un-loaded HANs, (b) MD-CPT/HANs were observed at the 1st day, and (c) at the 28th day. (E) In vitro release profiles of MD-CPT/HANs and MD-CPT suspension in PBS (pH 7.4) for 8 h (n = 3). (For interpretation of the references to color in this figure legend, the reader is referred to the web version of this article.)

software (SPSS version 13.0; SPSS, Inc., Chicago, IL). $P < 0.05$ was considered statistically significant.

3. Results and discussion

3.1. Preparation, characterization and surface morphology of HA nanoemulsion

Amphiphilic HA-GMS was synthesized by formation of ester linkages through an EDC/NHS mediated reaction protract the material's degradation and dissolution thereby improving its mechanical stability (Collins & Birkinshaw, 2013a), and form HANs with flexible structure, hydrophilic interface and hydrophobic interior by ultrasonic emulsification (Kong et al., 2011a,b). The hydrophobicity of MD-CPT made itself entrapped to vehicle interior. Different mass ratios of HA-GMS with MD-CPT gave rise to the differences of the particle size and zeta potential shown in Table 2. The HANs were physically stable with a nano-scale size, relatively narrow size distributions, and a negative charge. It was found that the particle size significantly ($P < 0.05$) increased from 160.1 ± 23.15 nm to 244.8 ± 12.68 nm and zeta potential absolute value decreased significantly ($P < 0.05$) with the relative increase of MD-CPT. The increase of hydrophobic drugs caused the increasing size of the hydrophobic core of nanoemulsions, the vesicular structure became loose and irregular, the relative proportion of the interface polar group decreased, and surface charge naturally decreased. The EE% (Entrapment efficiency) significantly ($P < 0.05$) decreased from $81.81 \pm 1.68\%$ to $65.23 \pm 6.71\%$, which was attributed to the saturation of the hydrophobic domain offered by HA-GMS The decrease of EE% might also be due to the leakage of the excessive drug from nanoemulsions. Flexible carriers like nanoemulsions are inclined to leak drug compared with rigid nanoparticles, which was also beneficial for drug release. The increasing amount of MD-CPT might lead to exposure of the hydrophobic domain, poor solubility and lack of systemic stability, which was apt to form aggregation in nanoemulsion. The optimization of the nanoemulsions preparation has been screened in the previous work (Kong et al., 2011a,b) to achieve an optimal proportion. As shown in Table 2, there was the minimum differences between 5:1 and 4:1 (m/m), particle size were less than 200 nm, zeta potential absolute value high than 14 mV, PdI with good value and EE% larger than 80% (All differences in values were less than 5%). Therefore drug loading capacity of 4:1 (m/m) was higher, which was adopted in subsequent research. The results above and TEM pictures shown in Fig. 2Ba/b demonstrated that both HANs and MD-CPT/HANs formed spherical morphology with good dispersion, and MD-CPT/HANs were larger than unloaded HANs.

The confocal laser scanning microscope (CLSM) study showed that the overlap of green fluorescence (FITC-HANs) and blue fluorescence (MD-CPT) gave rise to the cyan spots, indicated MD-CPT was successfully entrapped within HANs (Fig. 2C).

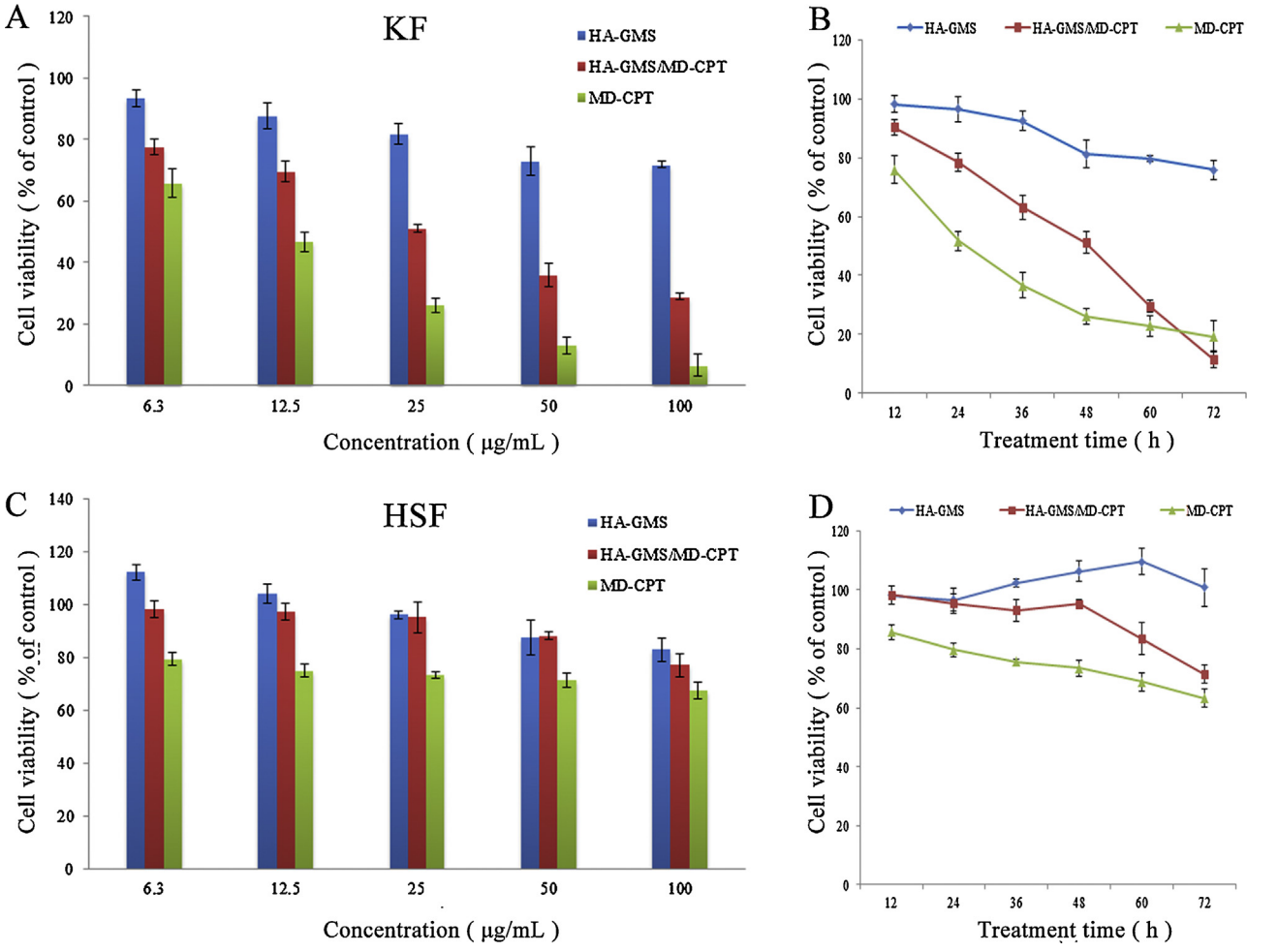

Fig. 3. In vitro cytotoxicity of HA-GMS, HA-GMS/MD-CPT and MD-CPT (DMSO as menstruum, V/V < 0.5%) with different concentration ((A)and (C)) and different treated time ((B) and (C)), Keloid fibroblasts and Human skin fibroblasts came from the same patients, 37 °C, incubated for 48 h, matching principle was equivalent to 4:1 (m/m) of HA-GMS: MD-CPT, the results represents as the means ± SD ($n = 6$).

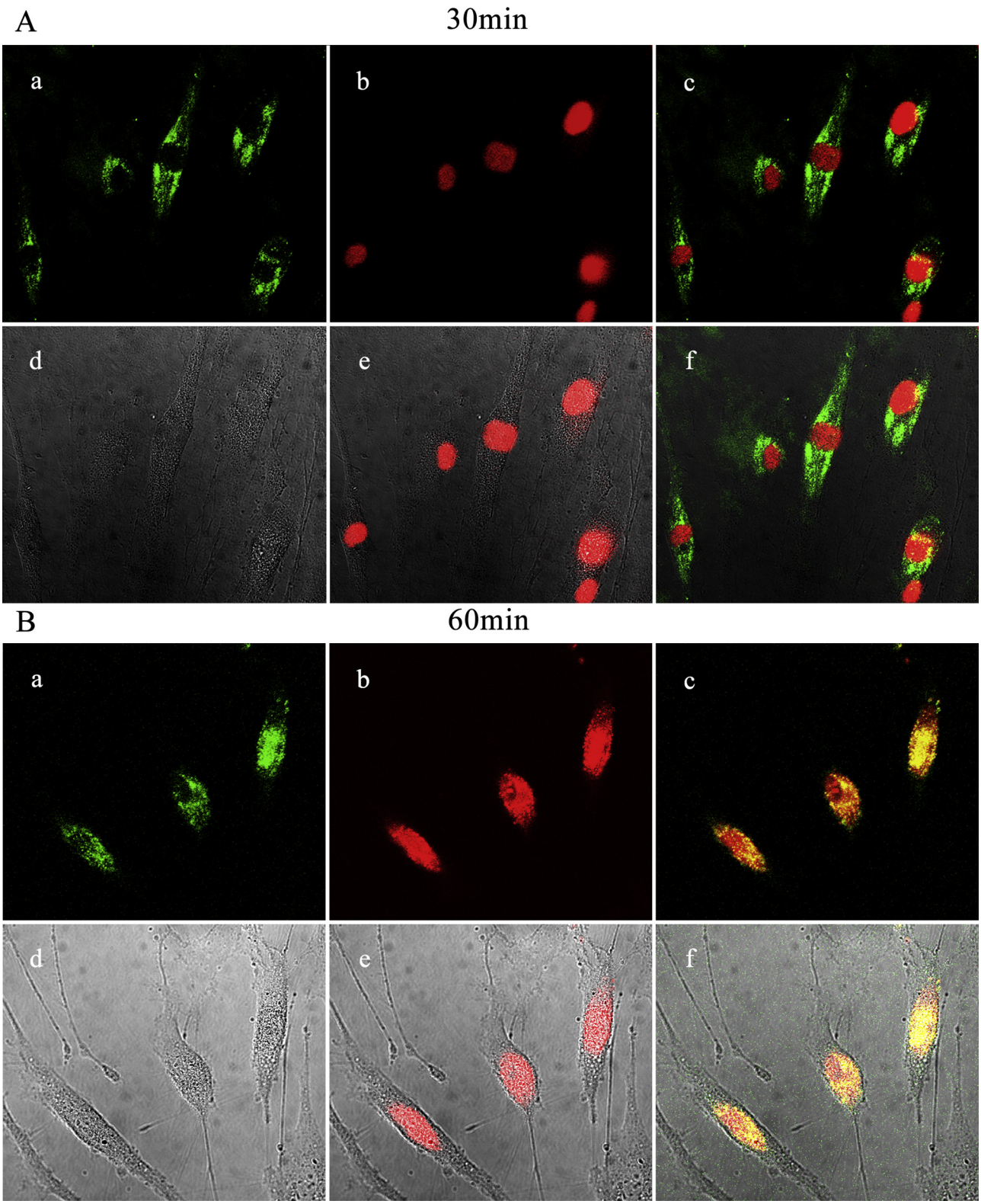

Fig. 4. CLSM images of Keloid fibroblasts with FITC-HANs at 37 °C for 30 min (A), 60 min (B) of incubation under different magnification (400×). (a) FITC-labeled HANs; (b) PI stained cell nucleus; (c) (a) and (b) merged; (d) bright field; (e) (b) and (d) merged; (f) overlapped image. (For interpretation of the references to color in this figure legend, the reader is referred to the web version of this article.)

Release profile of MD-CPT from HANs in vitro was performed by dialysis method in PBS (pH 7.4). HANM4 and HANM5 were formulations with high EE% (Table 2), MD-CPT suspension as control (Fig. 2E). The release curve of HANM4 is nearly linear, and release rate reached 87.15% after 8 h. This phenomenon could also be attributed to an effect of sustained drug released property (Table 3).

Stability and in vitro drug release were essential for HANs as a transdermal carrier. The stability of HANs was monitored during

Table 2
Zeta potential, particle size, polydispersity index (PdI) and EE% of HA-GMS NPs.

Formulation code	HA-GMS to MD-CPT (m/m)	Particle size (nm)	Zeta potential (mV)	PdI	EE%
–	Un-load HANs	75.7 ± 14.87	−16.2	0.33	–
HANM5	5:1	160.1 ± 23.15	−15.6	0.55	81.81 ± 1.68
HANM4	4:1	175.1 ± 13.83	−14.2	0.49	80.68 ± 1.71
HANM3	3:1	214.2 ± 10.15	−10.6	0.55	77.85 ± 1.29
HANM2	2:1	237.6 ± 4.53	−9.1	0.38	71.22 ± 3.37
HANM1	1:1	244.8 ± 12.68	−9.6	0.54	65.23 ± 6.71

The mass ratios of HA-GMS to MD-CPT were from 5 to 1. Data represented the mean ± SD, $n = 3$.

storage of 28 days at 4 °C, the mass ratio of HA-GMS to MD-CPT was 4:1. The particle size increased and absolute value of zeta potential decreased with time (Fig. 2A). Even though the tendency was inevitable that was determined by nature, nanoemulsions showed not much variation in size and maintained spherical with good dispersion (Fig. 2B and Dc). The results suggested that the MD-CPT/HANs had desirable stability and favorable controlled release for MD-CPT.

3.2. Cytotoxicity in vitro

Keloid fibroblasts (KF) are closely related with keloid growth, spread, infiltration the surrounding tissue, and fibrosis (Bayat et al., 2005), which therefore were taken as model and underwent exposure to treatment groups of MD-CPT, HA-GMS itself without surfactants (Kong et al., 2013) and HA-GMS/MD-CPT. According to MTT survival assays (Fig. 3A), both treated groups (MD-CPT

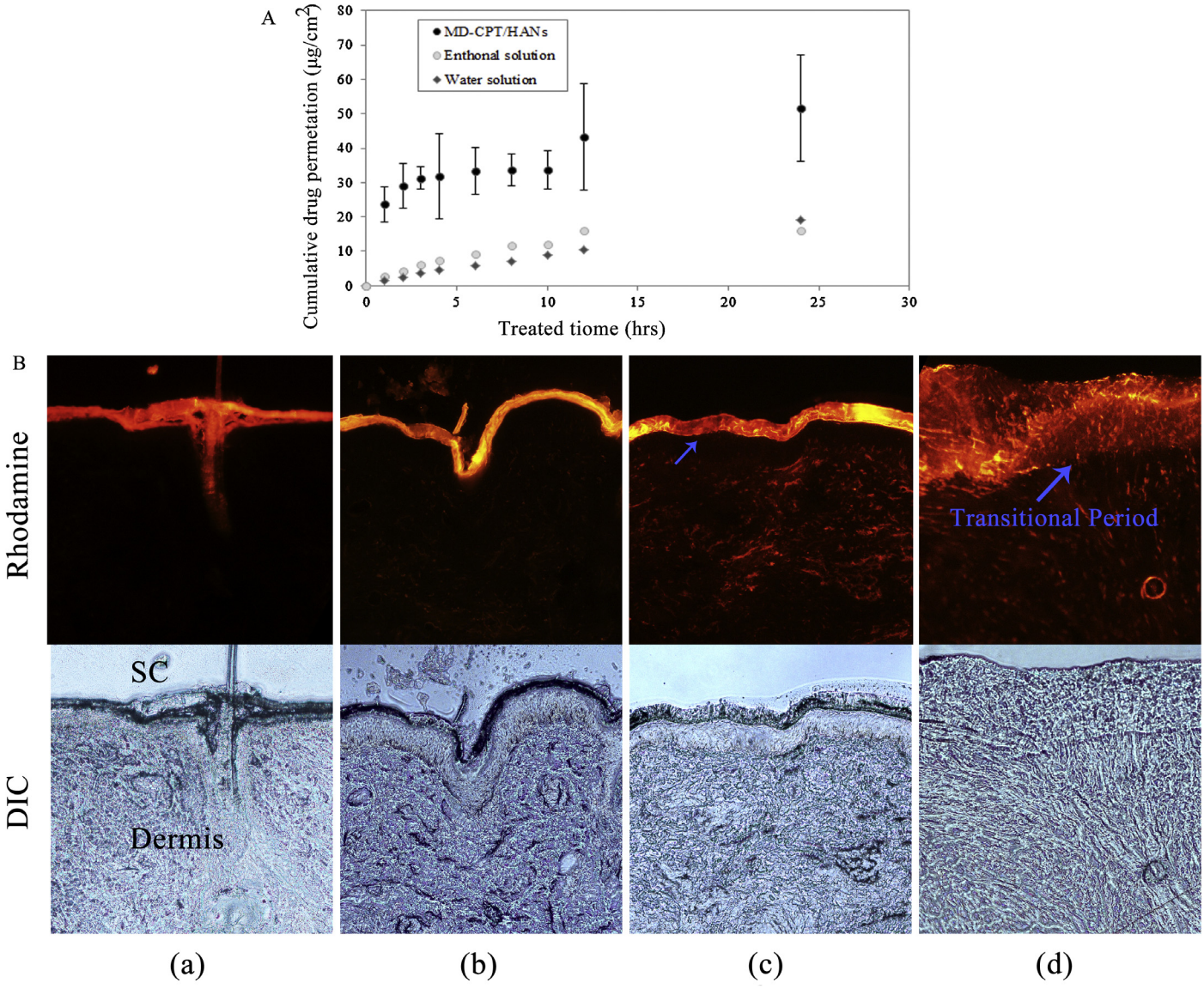

Fig. 5. A Permeation profiles of MD-CPT through the excised rat full skin from 1.0 mg/mL HANs (MD-CPT: 0.25 mg/mL). The control samples were ethanol solution of MD-CPT (0.25 mg/mL) and water solution (0.5% DMSO as solution medium; 0.25 mg/mL) (Mean ± SD, $n = 3$) (B). Penetration of rhodamine labeled MD-CPT/HANs into human Keloid skin. (a) At the beginning (<5 min): Control (100×). (b) After 4 h exposure (100×). (c) After 24 h exposure (50×). (d) The transition of HANs loaded the drug MD-CPT permeating skin across stratum corneum and diffusing deeper into dermis. The blue arrow points (200×). (For interpretation of the references to color in this figure legend, the reader is referred to the web version of this article.)

Table 3
In vitro percutaneous permeation parameters of MD-CPT in HANs and solution form through excised rat dorsal skin (mean ± SD, $n = 3$).

Formulation[a]	Jss (μg/(cm² h))	Kp ($\times 10^{-3}$ cm/h)	Qt/S (μg/cm²)
HANM4[b]	12.53 ± 0.39	12.53 ± 0.39	51.70 ± 15.51
Ethanol solution	0.67 ± 0.03	0.67 ± 0.03	16.07 ± 1.21
Water solution	0.75 ± 0.02	0.75 ± 0.02	19.07 ± 0.33

[a] Concentration of MD-CPT was 0.25 mg/mL.
[b] HANM4 (HA-GMS to MD-CPT (m/m) of MD-CPT/HANs was 4:1).

and HA-GMS/MD-CPT) significantly ($P < 0.05$) increased cytotoxicity in primary KF ($n = 10$) and HSF ($n = 6$) with the increase of the concentration. The growth inhibition rates were 34.33 ± 4.67% and 25.52 ± 2.53% at the concentration 6.3 μg/mL of MD-CPT, and IC_{50} was 10.67 μg/mL and 25.13 μg/mL, respectively. Moreover, the inhibition to KF was dose-dependent. The HA-GMS/MD-CPT-treated groups exhibited lower cytotoxicity than the groups treated with MD-CPT in KF (Fig. 3A/B). The phenomenon was probably attributed to the fact that MD-CPT mixed partially with HA-GMS overnight. The polyhydroxyl structure of HA, the open state lactone ring of MD-CPT in medium and the hydrophobic domain of monostearin (glycerol α-monostearate, GMS) might interact with each other and wrap into temporary and unstable complexes. The large size of complexes hampered them from entering cells. However, MD-CPT/HA-GMS still exhibited a good inhibitory effect.

The inhibition to KF was also time-dependent (Fig. 3B). The cell viability of the treated group (MD-CPT) sharply decreased 48 h before, the downtrend slowed down as follow. However, KFs treated with MD-CPT/HA-GMS, the cell viability decreased linearly with time, which demonstrated a controlled-release efficacy, and finally reached its lowest point 11.4 ± 2.9%, lower than 19.3 ± 5.3% (MD-CPT). MD-CPT/HA-GMS showed a favorable anti-proliferation efficacy with time.

Compared with KF, MD-CPT was no dose-dependent, weak time-dependent and less toxic against HSF (Fig. 3C/D), it was concluded that MD-CPT was highly selective and effective for KF and less effective for HSF, which was consistent with that the CPT-induced apoptosis was selective to hyperplastic cells as G1/S Cell Cycle Blockers (Park et al., 1997; Adams et al., 2006). In contrast, HA-GMS/MD-CPT did not show severe inhibitory activity, and alleviated the toxicity, which played a protective effect. The proliferation of KF could be inhibited, while there was no obvious damage to normal cells. This property was beneficial for treatment of keloid.

3.3. Cellular uptake of MD-CPT/HANs into keloid fibroblasts in vitro

Cellular uptake of MD-CPT/HANs into KF was the key to achieve the inhibition of cell proliferation. The internalization and localization of MD-CPT/HA into KF were examined by CLSM. Fig. 4A presented the process of MD-CPT loaded FITC-HANs were gradually internalized into KF. The time dependence attributed to cellular uptake was a dynamic process which was supposed to have been endocytosing until equilibrium. The images showed the uptake of FITC-HANs by KFs (Fig. 4). The distribution of FITC-HANs in cells was observed under magnification (400×). FITC-HANs had been endocytosed at 30 min and mainly concentrated in the cytoplasm and dispersed in the whole space outside the nuclear, which displayed blank black holes (Fig. 4Aa; 400×). The green fluorescence of FITC-HANs merged with the red fluorescence of PI-stained nucleus (Fig. 4Ac), and the division was clear. HANs did not penetrate into the nucleus. After 60 min, part of FITC-HANs entered into nuclear area, and the FITC-HANs in the cytoplasm was obviously reduced, and nearly disappeared (Fig. 4B). Both strong red and green fluorescence are observed in the nucleus, overlapped to yellow, which implies that HANs penetrated into the nucleus. The outline of cells

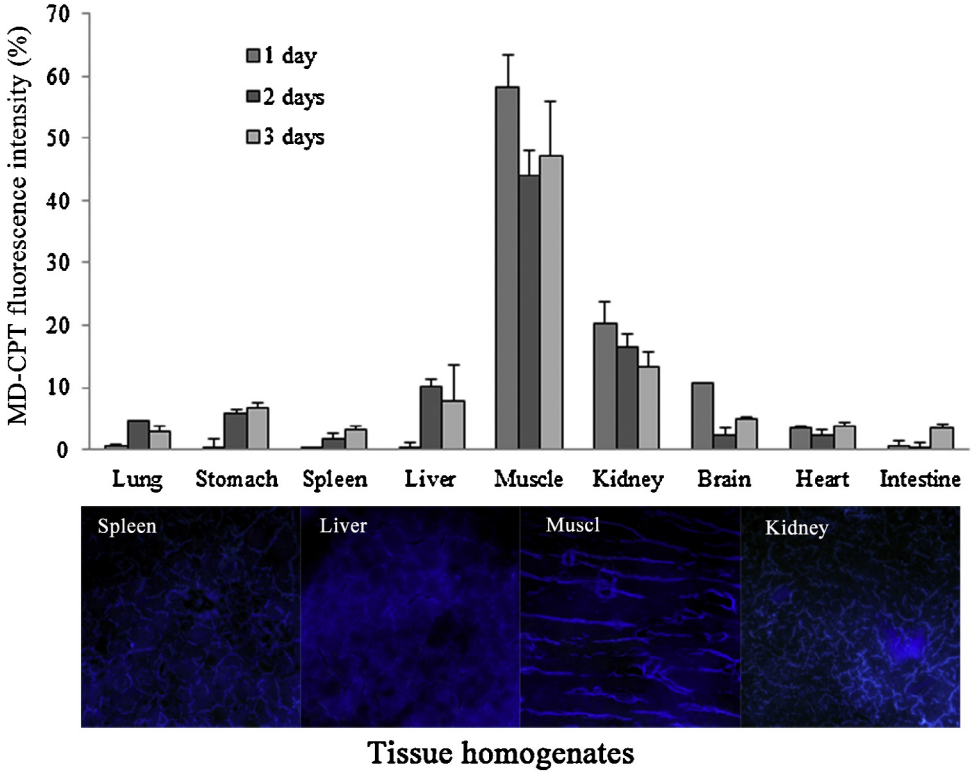

Fig. 6. Tissue distribution of MD-CPT/HANs was measured with the fluorescence intensity (emitted by MD-CPT) 1, 2 and 3 days after transdermal delivered to rats. Data are represented as means ± SD; tissue accumulation of MD-CPT/HANs after 3 days through transdermal delivered to rats measured by fluorescence microscopy (100×): spleen, liver, kidney and muscle.

was also very clear under light microscopy (Fig. 4Ad/Bd). These fluorescent microscopic photos provide direct evidence of cellular uptake, and exhibit HANs' good ability in endocytosis.

3.4. Transdermal drug permeation study

3.4.1. Ex vivo quantitative studies of transdermal drug permeation

Transdermal drug permeation of MD-CPT/HANs was studied quantitatively across rat skin using Franz diffusion cell. MD-CPT ethanol solution (0.25 mg/mL) and water solution (0.25 mg/mL; 0.5% DMSO as solution medium) was taken as control groups and PBS (pH 7.4) as receptor isotonic solution. As shown in Fig. 8, over 24 h exposure, the cumulative drug permeation (Qt, μg/cm^2) through the skin showed sigmoid curve. At 1 h, the Qt of MD-CPT was 23.62 ± 4.79 μg/cm^2, and reached to the temporary saturation point at 6 h. The increment of Qt seemed to dramatically slow down after 6 h, went forward to grow after 12 h, and finally reached to 51.70 ± 9.51 μg/cm^2 at the end of 24 h. This value is substantially higher than the control groups (Fig. 5A). For HANs, the steady-state fluxes (J_{ss}, 2.15 ± 0.39 μg/cm^2) was significantly ($P < 0.05$) higher than the control groups. MD-CPT/HANs showed a favorable percutaneous permeability.

3.4.2. Ex vivo qualitative studies of transdermal drug permeations

Fluorescence microscope photos provided a dynamical permeation process. The Red fluorescence emitted by rhodamine labeled MD-CPT/HANs gradually permeated into skin and mainly concentrated in the stratum corneum (SC) after 4 h exposure (Fig. 5Bb). After 24 h treatment, the red fluorescence provided direct evidences of percutaneous penetration, verifying the successful permeation of HANs across SC layer and deeper diffusion into dermis (Fig. 5Bc). Meanwhile the concentration at the SC gradually reduced and the boundary between the epidermis and SC became dull at the interface (The blue arrow points in Fig. 5Bd). These pictures directly verify HANs could transport MD-CPT through the epidermis and then into the dermal lesion area of keloid. Even though photos exhibited the successful transdermal process, the effect was not obvious compared with the quantitative study above. Because human keloid skin is different from normal skin, the accumulation of extracellular matrix and especially excessive collagen deposition lead to severe skin fibrosis. Meanwhile, the capillary

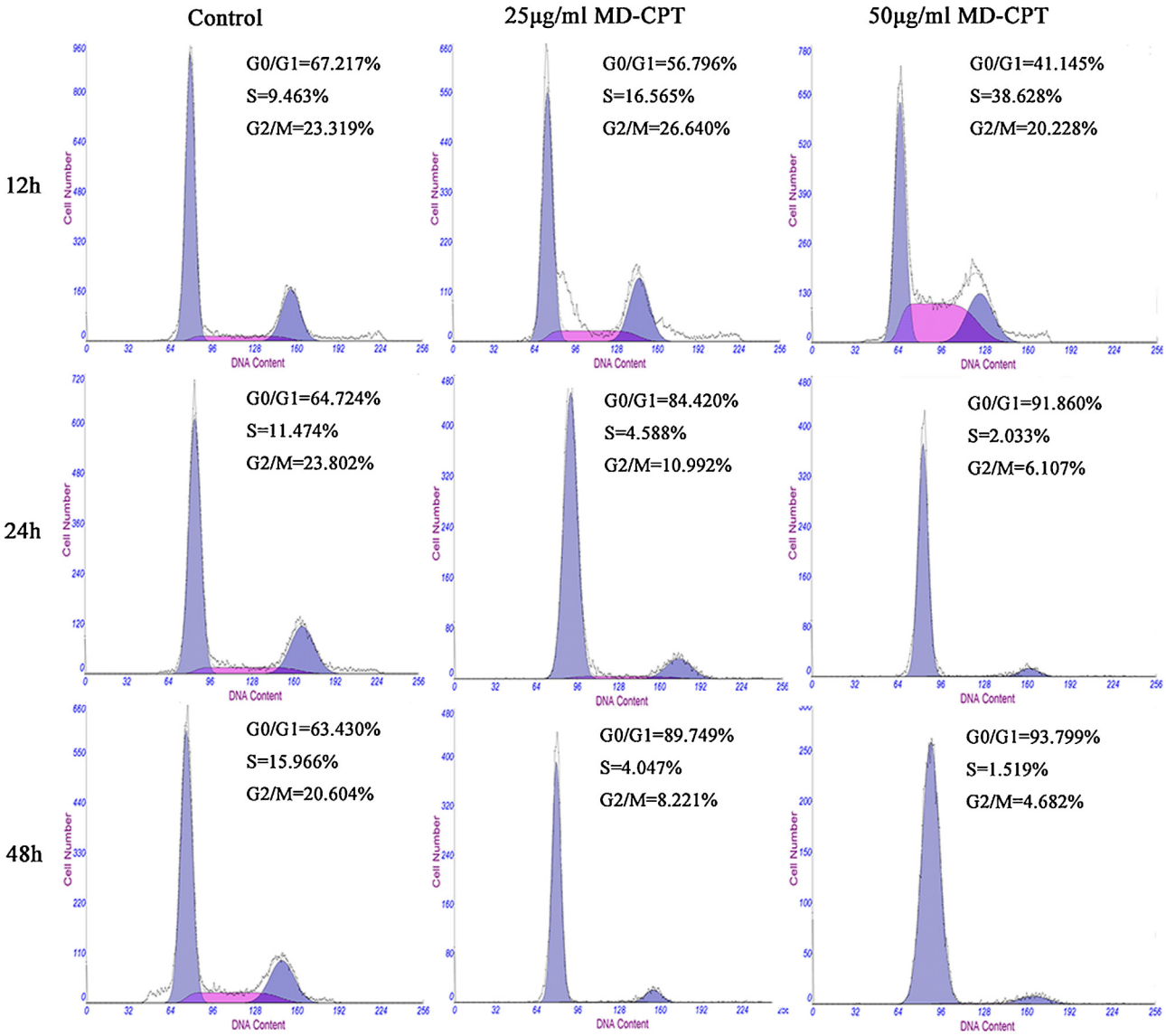

Fig. 7. Flow cytometry histograms representing cell cycle distributions of keloid fibroblasts treated with MD-CPT/HANs 25 μg/mL, 50 μg/mL (drug relative concentration in the medium) or controls without treatment at 37 °C for 12, 24, 48 h of incubation. G0/G1 phase cell cycle arrest appeared in response to MD-CPT/HA MD-CPT/HA therapy.

vessel disappears gradually, corneous layer becomes thicker, and keloid local presents an approximate enclosed area (Shih & Bayat, 2010), which increases the difficulty of permeation and diffusion.

Based on the small size, bioactive properties and high encapsulation capacity of MD-CPT, HANs successful permeated across SC layer and deeper diffusing into dermis with MD-CPT. Due to the permeability of a substance through the skin is related to its size under certain conditions and osmotic pressure formed by the substance on the skin surface (Kong & Park, 2011). HA possesses many properties including specific hydration, viscoelasticity, lubrication and biocompatibility, which help enable it to absorb water and preserve moisture (Garg & Hales, 2004). The higher permeation rate from HANs is based on the HA capability for a spontaneous skin penetration via transdermal hydration gradient and from high lipid hydration energy. The lipid hydrophilicity leads to xerophobia, a tendency to avoid dry surroundings and causes carriers sitting near or at the skin surface to resist dehydration. In order to remain maximally swollen HANs thus try to follow the local hydration gradients and thereby get into deeper and better hydrated skin strata. A spontaneous drug carrier and drug transport in the desired direction, from the dry skin surface toward the better hydrated skin interior, may result from this. Thus of HANs showed nearly 12 to 12 folds better skin permeation of MD-CPT than drug ethanol solution due to deformability and the ability to retain vesicle integrity.

3.5. Tissue distribution assays in vivo

In order to further verify the percutaneous penetration of MD-CPT/HANs, their diffusion into systemic circulation and accumulation in organs and tissues, living rats transdermal delivery model was used (Fig. 1). The data were normalized with the negative control, the tissues from rats without treatments. The background fluorescence from these tissues was subtracted from the experimental tissue fluorescence. The percentage of MD-CPT detected was expressed as the ratio of the fluorescence intensity of each tissue relative to the sum of fluorescence intensity of all tissues analyzed.

It demonstrated that MD-CPT/HANs were distributed mainly in the muscle excised under the dosing skin area ($47.17 \pm 8.66\%$), followed by the kidney ($13.33 \pm 1.88\%$), spleen ($9.32 \pm 0.45\%$) and liver ($7.98 \pm 5.74\%$) after 3 days, which was further verified by fluorescence microscopy pictures in Fig. 6. The high content in muscle tissue benefit to the drug reversing osmosis to the dosing skin area so as to prolong the efficacy of drug. The accumulation of the gastrointestinal tract, brain and heart were significant lower ($P < 0.05$), all below 10%. It suggests that the toxicity of MD-CPT was controlled and limited by HANs. And the rapidly dividing normal cells sensitive to MD-CPT were protected, including cells in the gastrointestinal tract, bone marrow cells and hair follicles. The exist of MD-CPT in liver, spleen and kidney showed it had gone into the systemic circulation, and entered the metabolism, and excreted from the body finally.

3.6. Cell cycle regulation in vitro

The inhibitory properties of MD-CPT were further studied upon the cell cycle regulation using flow cytometry. The number of cells at each cell cycle phase was determined. The percentages of cells at G0/G1 phase increased with the concentration of MD-CPT (mixed with HA-GMS) and treatment time. It was demonstrated that MD-CPT triggered G1/S phase arrest. After treated 12 h, the cells at S phase firstly increased from 9.467% to 38.628% (Fig. 7). As the extension of treated time, the cells at both S and G2/M phase apparently decreased. The total number

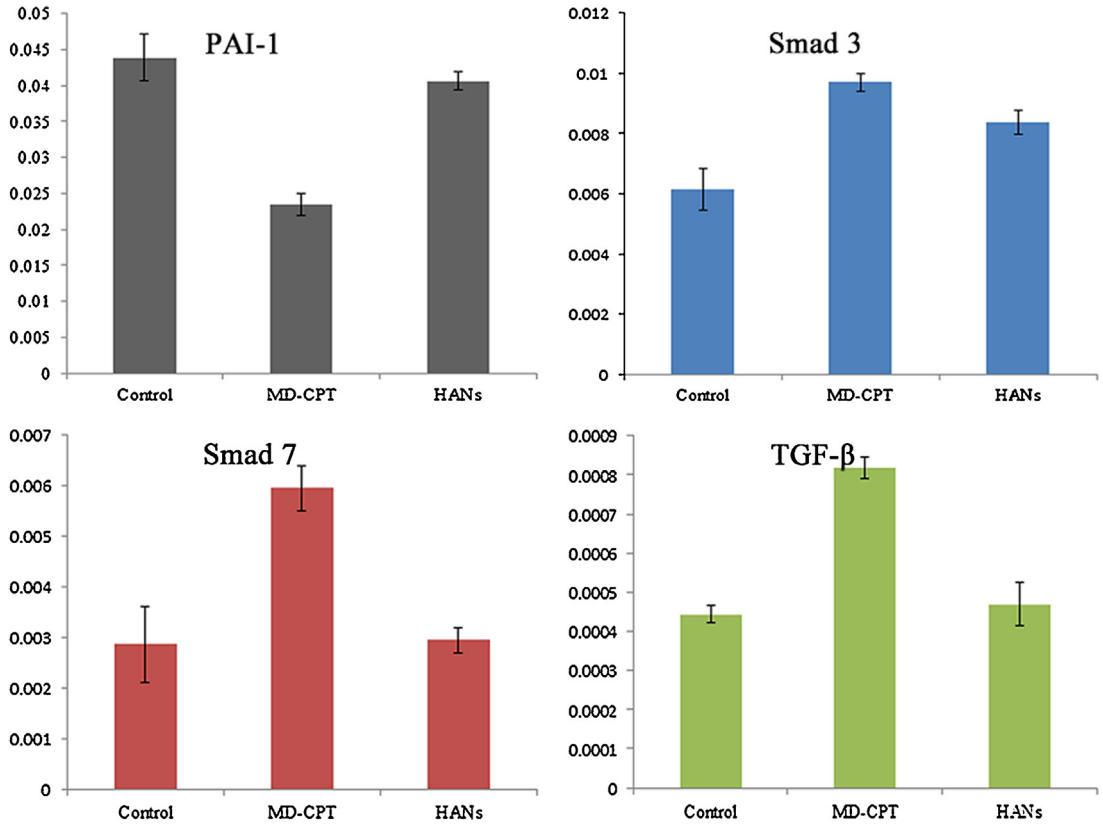

Fig. 8. Gene express of PAI-1(blank), Smad3 (blue), Smad7 (red) and TGF-β (green). *Y*-axis showed $2^{-\Delta Ct}$. ΔCt = target gene Ct − reference gene Ct, each sample for each gene was measured with three times repeat. (For interpretation of the references to color in this figure legend, the reader is referred to the web version of this article.)

of viable cells also decreased, more than 90% cells suspended at G0/G1 phase. KF showed a tendency of cellular aging and apoptosis. These results indicated that addition of MD-CPT contributed to cell cycle arrest and prevented it further into mitosis. The conclusion was in agreement with the cytotoxicity examination.

3.7. Gene expression regulation in vitro

Plasminogen activator inhibitor-1 (PAI-1) is a major effector and downstream target of transforming growth factor-β (TGF-β) in the progress of several clinically important fibrotic disorders, which is highly up-regulated in Keloid and causatively linked to disease severity. It has been verified that knockdown of PAI-1 significantly reduced keloid, and reduced collagen-I and -III at both mRNA and protein levels. SMAD pathway is required for PAI-1 induction by TGF-β (Samarakoon, Overstreet, Higgins, & Higgins, 2012; Syed et al., 2013). As shown in Fig. 8, MD-CPT significantly ($P < 0.05$) down-regulated PAI-1, preliminarily demonstrated that MD-CPT was beneficial to inhibit keloid. It is noted that, TGF-β and Smad3 was up-regulated, which were adverse to the principle of transcriptional regulation of TGF-β/SMAD signal pathway. It was presumed that some inhibitor may obstruct TGF-β/SMAD pathway. SMAD2/3 activation increases in keloid. However, Smad7 blocks Smad2/3 binding to TβRI or form oligomerization with Smad4 (Akhurst & Derynck, 2001). Therefore the up-regulated Smad7 might prevent TGF-β from stimulating PAI-1 expression, and then inhibit the progress of keloid induced by fibrotic disorders.

4. Conclusion

HA nanoemulsions successfully loaded MD-CPT with good stability and favorable controlled-released property. Their nanoparticle size, negative charge, flexible structure and hydrophilic interface facilitated transdermal permeation. HANs as transdermal carriers were verified to transfer MD-CPT into the corium layer of human keloid skin and performed desirable skin permeable capacity. MD-CPT/HANs was endocytosed by keloid fibroblast, played a dose-dependent inhibitory effect to KF, but not to normal skin fibroblast. The growth-inhibitory effect was further clarified upon cell cycle regulation, which arrested cells at G1/S and prevented them entry into mitosis. At last, MD-CPT induced the significantly down-regulation of PAI-1 and up-regulation of Smad7, which was potential to prevent fibrosis and inhibit keloid. The nanocarrier guided MD-CPT into the systemic circulation, entered the metabolism and avoided its damage to gastrointestinal tract, heart, and brain. The study suggested that MD-CPT/HANs as transdermal delivery system for keloid inhibition has potential to be used for keloid therapy.

Acknowledgments

This work was supported by a grant from International S&T Cooperation Program of China (2013DFG32880), The National Natural Science Foundation of China (31000423, 31300786) and Doctoral Fund of Ministry of Education of China (20120132110012).

References

Adams, D. J., Wahl, M. L., Flowers, J. L., Sen, B., Colvin, M., Dewhirst, M. W., & Wani, M. C. (2006). Camptothecin analogs with enhanced activity against human breast cancer cells. II. Impact of the tumor pH gradient. *Cancer Chemotherapy and Pharmacology*, *57*(2), 145–154.

Akhurst, R. J., & Derynck, R. (2001). TGF-β signaling in cancer-a double-edged sword. *Trends in Cell Biology*, *11*, S44–S51.

Bagabir, R., Syed, F., Paus, R., & Bayat, A. (2012). Long-term organ culture of keloid disease tissue. *Experimental Dermatology*, *21*(5), 376–381.

Bayat, A., Arscott, G., Ollier, W. E. R., Mc Grouther, D. A., & Ferguson, M. W. J. (2005). Keloid disease: Clinical relevance of single versus multiple site scars. *British Journal of Plastic Surgery*, *58*(1), 28–37.

Chaudhary, H., Kohli, K., & Kumar, V. (2013). Nano-transfersomes as a novel carrier for transdermal delivery. *International Journal of Pharmaceutics*, *454*(1), 367–380.

Collins, M. N., & Birkinshaw, C. (2013a). Hyaluronic acid solutions—A processing method for efficient chemical modification. *Journal of Applied Polymer Science*, *130*(1), 145–152.

Collins, M. N., & Birkinshaw, C. (2013b). Hyaluronic acid based scaffolds for tissue engineering—A review. *Carbohydrate Polymers*, *92*(2), 1262–1279.

Ganesh, S., Iyer, A. K., Morrissey, D. V., & Amiji, M. M. (2013). Hyaluronic acid based self-assembling nanosystems for CD44 target mediated siRNA delivery to solid tumors. *Biomaterials*, *34*(13), 89–3502.

Garg, H. G., & Hales, C. A. (2004). *Chemistry and biology of hyaluronan*. London: Elsevier Science & Technology Books.

Gorain, B., Choudhury, H., Kundu, A., Sarkar, L., Karmakar, S., Jaisankar, P., & Pal, T. K. (2014). Nanoemulsion strategy for olmesartan medoxomil improves oral absorption and extended antihypertensive activity in hypertensive rats. *Colloids and Surfaces B: Biointerfaces*, *115*, 286–294.

Hariri, G., Edwards, A. D., Merrill, T. B., Greenbaum, J. M., Van der Ende, A. E., & Harth, E. (2013). Sequential targeted delivery of paclitaxel and camptothecin using a cross-linked nanosponge network for lung cancer chemotherapy. *Molecular Pharmaceutics*, *11*(1), 265–275.

Kano, Y., Suzuki, K., Akutsu, M., Suda, K., Indue, Y., Yosnida, M., & Miura, Y. (1992). Effects of CPT-11 in combination with other anti-cancer agents in culture. *International Journal of Cancer*, *50*(4), 604–610.

Kong, M., & Park, H. J. (2011). Stability investigation of hyaluronic acid based nanoemulsion and its potential as transdermal carrier. *Carbohydrate Polymers*, *83*(3), 1303–1310.

Kong, M., Chen, X. G., & Park, H. J. (2011). Design and investigation of nanoemulsified carrier based on amphiphile-modified hyaluronic acid. *Carbohydrate Polymers*, *83*(2), 462–469.

Kong, M., Chen, X. G., Kweon, D. K., & Park, H. J. (2011). Investigations on skin permeation of hyaluronic acid based nanoemulsion as transdermal carrier. *Carbohydrate Polymers*, *86*(2), 837–843.

Kong, M., Park, H., Feng, C., Hou, L., Cheng, X., & Chen, X. (2013). Construction of hyaluronic acid noisome as functional transdermal nanocarrier for tumor therapy. *Carbohydrate Polymers*, *94*, 634–641.

Li, K., Pan, J., Feng, S. S., Wu, A. W., Pu, K. Y., Liu, Y., & Liu, B. (2009). Generic strategy of preparing fluorescent conjugated-polymer-loaded poly(DL-lactide-*co*-glycolide) nanoparticles for targeted cell imaging. *Advanced Functional Materials*, *19*(22), 3535–3542.

O'Connor, P. M., Nieves-Neira, W., Kerrigan, D., Bertrand, R., Goldman, J., Kohn, K. W., & Pommier, Y. (1991). S-phase population analysis does not correlate with the cytotoxicity of camptothecin and 10,11-methylenedioxycamptothecin in human colon carcinoma HT-29 cells. *Cancer Communications*, *3*(8), 233–240.

Park, D. S., Morris, E. J., Greene, L. A., & Geller, H. M. (1997). G1/S cell cycle blockers and inhibitors of cyclin-dependent kinases suppress camptothecin-induced neuronal apoptosis. *The Journal of Neuroscience*, *17*(4), 1256–1270.

Samarakoon, R., Overstreet, J. M., Higgins, S. P., & Higgins, P. J. (2012). TGF-β1 → SMAD/p53/USF2 → PAI-1 transcriptional axis in ureteral obstruction-induced renal fibrosis. *Cell and Tissue Research*, *347*(1), 117–128.

Shih, B., & Bayat, A. (2010). Genetics of keloid scarring. *Archives of Dermatological Research*, *302*(5), 319–339.

Sun, Y., Wang, L., Sun, S., Liu, B., Wu, N., & Cao, X. (2008). The effect of 10-hydroxycamptothecine in preventing fibroblast proliferation and epidural scar adhesion after laminectomy in rats. *European Journal of Pharmacology*, *593*(1), 44–48.

Supko, J. G., & Malspeis, L. (1993). Pharmacokinetics of the 9-amino and 10,11-methylenedioxy derivatives of camptothecin in mice. *Cancer Research*, *53*(13), 3062–3069.

Syed, F., Bagabir, R. A., Paus, R., & Bayat, A. (2013). Ex vivo evaluation of antifibrotic compounds in skin scarring: EGCG and silencing of PAI-1 independently inhibit growth and induce keloid shrinkage. *Laboratory Investigation*, *93*(8), 946–960.

Tanizawa, A., Kohn, K. W., Kohlhagen, G., Leteurtre, F., & Pommier, Y. (1995). Differential stabilization of eukaryotic DNA topoisomerase I cleavable complexes by camptothecin derivatives. *Biochemistry*, *34*(21), 7200–7206.

Tuan, T. L., & Nichter, L. S. (1998). The molecular basis of keloid and hypertrophic scar formation. *Molecular Medicine Today*, *4*(1), 19–24.

Yang, K., Gao, T. T., Bao, Z. X., Su, J., & Chen, X. G. (2013). Preparation and characterization of a novel thermosensitive nanoparticle for drug delivery in combined hyperthermia and chemotherapy. *Journal of Materials Chemistry B*, *1*(46), 6442–6448.